

Light-assisted small molecule screening against protein kinases

Álvaro Inglés-Prieto¹, Eva Reichhart¹, Markus K. Muellner², Matthias Nowak¹, Sebastian M. Nijman^{2,4}, Michael Grusch³ & Harald Janovjak^{1,*}

¹ Institute of Science and Technology Austria (IST Austria), 3400 Klosterneuburg, Austria.

² CeMM-Research Center for Molecular Medicine of the Austrian Academy of Sciences, 1090 Vienna, Austria.

³ Institute of Cancer Research, Department of Medicine I, Comprehensive Cancer Center Vienna, Medical University of Vienna, 1090 Vienna, Austria.

⁴ Present address: Ludwig Institute for Cancer Research, NDM Research Building, Roosevelt Drive, Headington, Oxford OX3 7XR, United Kingdom.

* e-mail: harald@ist.ac.at

Abstract

High-throughput live-cell screens are intricate elements of systems biology studies and drug discovery pipelines. Here, we demonstrate an optogenetics-assisted method that obviates the addition of chemical activators and reporters, reduces the number of operational steps and increases information content in a cell-based small molecule screen against human protein kinases including an orphan receptor tyrosine kinase. This blueprint for all-optical screening can be adapted to many drug targets and cellular processes.

Main text

Over the past decades, many chemical processes have been improved by replacing additives, such as catalysts, initiators or emulsifiers, with physical stimuli, such as light or ultrasound¹⁻⁴. Although replacement results in reduced cost, increased robustness and improved sustainability, this general principle has not found many adaptations in chemical biology. Automated screens using living cells are essential in the identification and characterization of small molecules that act on disease-related proteins and cellular pathways. However, in many cell-based screens the need to add reagents that alter or report on cell activity results in complex operational design, high cost and sources of error. Furthermore, mammalian cells are sensitive to environmental perturbations (e.g. temperature or ionic strength) and subject to inherent variability. In neurobiology and cell biology, optogenetics and photopharmacology have recently harnessed the power of light to manipulate the behavior of cells and animals non-invasively and with high spatial and temporal precision⁵⁻⁷. Here, we developed an optogenetics-assisted, cell-based screening method that interrogates receptor tyrosine kinases (RTKs) and the mitogen-activated protein kinase/extracellular signal-regulated kinase (MAPK/ERK) pathway comprising one G-protein (Ras) and three intracellular kinases (Raf, MEK and ERK). We demonstrate that in this screening method the use of light for activation *and* detection of cell signaling obviated the need for addition of reagents, limited the number of operational steps and provided new strategies to increase specificity and counter variability.

The MAPK/ERK pathway is activated by RTKs and regulates cell survival, proliferation and differentiation. Modulators of the MAPK/ERK pathway, RTKs and other protein kinases are pursued as new therapeutics in cancer and metabolic and neurodegenerative disorders. We first engineered human embryonic kidney 293 (HEK293) cells that contain light-activated RTKs and a genetic fluorescent MAPK/ERK pathway reporter (**Fig. 1a**). The light-activated RTKs (also called 'Opto-RTKs') are modified growth factor receptors that are insensitive to their natural ligands but activated by blue light-induced homodimerization through incorporation of the light-oxygen-voltage-sensing (LOV) domain of aureochrome1 from *V. frigida*⁸ (**Supplementary Results, Supplementary Fig. 1**). We initially employed two Opto-RTKs, the light-activated murine fibroblast growth factor receptor 1

(Opto-mFGFR1) and the light-activated human epidermal growth factor receptor (Opto-hEGFR). In the fluorescent reporter (SRE-GFP), tandem repeats of serum response element (SRE)⁹, an enhancer sequence responsive to signaling pathways including the MAPK/ERK pathway, precede a gene coding for the green fluorescent protein (GFP). The engineered cells respond to light at a wavelength and intensity suited for Opto-RTK activation ($\lambda \sim 470$ nm, intensity ~ 200 $\mu\text{W}/\text{cm}^2$) with increased production of GFP (**Fig. 1b** and **Supplementary Fig. 2**), and combining Opto-RTKs and GFP reporter thus enables a novel 'all-optical' mode of operation where light was used to activate as well as read cellular signaling. Using this mode of operation, we were able to screen small molecules in the 384-well plate format without addition of reagents to induce or detect pathway activation and with few handling steps (**Fig. 1c** and **Supplementary Fig. 3**). This assay was robust (Z' -factor ≥ 0.7 , **Materials and Methods**) and not influenced by ambient light (**Supplementary Fig. 4**) or bleaching (**Supplementary Fig. 5**). In addition, all wells in the 384-well plate were activated at the same time and with nearly identical intensity using light emitting diodes (LEDs) (deviation of intensity $< 0.05\%$ over the plate, day-to-day variability $< 0.05\%$). In a set of kinase inhibitors (**Supplementary Table 1**), three molecules inhibited the mFGFR1-MAPK/ERK-axis by $> 50\%$, and these molecules are known kinase inhibitors of FGFR1 or of MAPK/ERK pathway components (**Fig. 1c, d** and **Supplementary Fig. 6**). To demonstrate the ability to identify whether ligands act at the receptor or downstream pathway, we conducted the same screen with Opto-hEGFR. Unlike FGFR1, which couples to the MAPK/ERK pathway *via* additional FGFR substrate adaptor proteins, EGFR directly activates it. Three molecules inhibited the EGFR1-MAPK/ERK-axis, and these molecules are known kinase inhibitors of EGFR or pathway components (**Fig. 1d**). Because inhibitors of FGFR1 were not detected in the screen with EGFR and *vice versa*, the method selectively identified those small molecules that specifically act on receptors or common downstream proteins. Collectively, these results demonstrate a cell-based small molecule screen in the 384-well format assisted by optogenetics. The method functions without added reagents and a reduced number of operational steps as physical contact to the living cells was not required.

Because peptides or other agonists are not required, the all-optical method can also screen against 'orphan' receptors, i.e. receptors for which native ligands are not known. To demonstrate optical control of an orphan receptor, we first identified human orphan RTKs through *de novo* database and bioinformatics analysis (**Supplementary Fig. 7**). The database search reported human ROS1 (hROS1), a proto-oncogene orphan RTK that is activated by protein fusion in a variety of tumor cell types^{10, 11}. To engineer a light-activated variant of human hROS1 (Opto-hROS1), we fused the dimerizing LOV domain to the intracellular domain of hROS1 (**Supplementary Fig. 8**). When testing the kinase inhibitor library against Opto-hROS1, we found three molecules that inhibited the hROS1-MAPK/ERK-axis (**Supplementary Fig. 9**). Two of these molecules (crizotinib and GSK-1120212) are known kinase inhibitors of hROS1 and pathway components. The third molecule (AV-951¹²) was active specifically against hROS1 but not mFGFR1 or hEGFR (**Supplementary Fig. 10**). Notably, AV-951 was previously not assigned to inhibit hROS1.

We next extended the method to increase information content in cell-based screens. First, we demonstrate that a second, spectrally-distinct FP (e.g. mKate2¹³) can be incorporated and detected separately from GFP (**Supplementary Fig. 10**). If expressed constitutively, this second protein can report small molecules that inhibit gene transcription and protein translation/folding¹⁴, potential assay confounders. As GFP exhibits fluorescence in the same wavelength range as many small molecules in screening collections, a red FP may generally improve assay performance. Second, we tested whether the ability to spatially focus activation can improve the method. Stimulation of optogenetic tools is often realized using custom-built hardware and continuous illumination¹⁵⁻¹⁷. However, microplate readers commonly part of screening platforms employ discontinuous flash lamps. We thus tested if flashes provide sufficient intensity to activate optogenetic proteins and found that 900 blue light flashes (2 μ s duration, 9 W average power of lamp) resulted in robust MAPK/ERK pathway activation in SPC212 cells expressing Opto-mFGFR1 (**Fig. 2a to c**). Using a light guide-lens assembly, we then confined flash lamp stimulation to the center of single wells (area~3.14 mm²) while leaving the well periphery unstimulated (**Fig. 2d, e**).

We thereby created two cell populations (activated center population and silent peripheral population) within each well, and we exploited these populations to obtain high-content measurements. When testing small molecules, we found that inactive molecules left centers *activated* and peripheries *silent*, inhibitory molecules resulted in *silent* centers and *silent* peripheries, and activators resulted in *activated* centers and *activated* peripheries (**Fig. 2f**). This result showed that probing two cell populations in a single well was sufficient to test for inhibitory or activating effects of a small molecule. In further experiments, one cell population may also serve as a local control for others. Because trial and control are performed under identical conditions in the same well, the influence of environmental perturbations on measurement outcome may be reduced. These experiments can be directly transferred to high-throughput platform microplate readers without the need for specialized instrumentation.

In summary, we demonstrate that incorporation of optogenetics enabled cell-based small molecule screens without additives but minimal operational steps and increased information content. Light acted as a universal ligand for receptors of different families (e.g. FGFR1, EGFR or ROS1), but, at the same time, was specific to stimulate the genetically-engineered receptors. Interference from endogenous receptors that may be also activated by added ligands can be excluded, which is particularly desirable when targeting receptors for which specific ligands are not available. For instance, in our experiments EGF or FGF2 will have bound to several receptor proteins expressed in these cells (FGFR1, FGFR2, FGFR3, FGFR-like 1 and EGFR), while Opto-RTK activation was specific to the engineered receptor. Activation by light may be in real-time to reveal new insights into molecular inhibition and cellular signaling mechanisms. For instance, the interaction between small molecules and proteins can be activation-state dependent^{18, 19}, and the duration and frequency of activation can determine choice of pathway or functional outcome^{20, 21}. The ability to switch signals on with temporal precision and tunable strength, even within one well, may explore these phenomena in a systematic and automated manner. This may be of particular use when exploring 'mutagenesis space' in genetic libraries and the method is compatible with transient cell transfection. We further foresee the extension and adaptation of this approach to other

drug targets to be straightforward because of an increasing number of available optogenetic tools and fluorescent reporters.

Acknowledgements

We thank M. Ernst for fruitful discussions, M. Spanova for technical assistance, R. Chait for photography, X. Amouretti and B. Harris for hardware specifications, R. Stahel (University of Zurich) for mesothelioma cells, and D.M. Chudakov (Shemiakin-Ovchinnikov Institute of Bioorganic Chemistry)/Evrogen (Moscow) for mKate2. This work was supported by grants of the European Union Seventh Framework Programme (CIG-303564 to H.J. and ERC-StG-311166 to S.M.N.), the Human Frontier Science Program (RGY0084_2012 to H.J.), and the Herzfelder Foundation (to M.G.). A.I.P. was supported by a Dan David fellowship and a Ramon Areces fellowship, and E.R. by the graduate program MolecularDrugTargets (W1232 Austrian Science Fund FWF) and a FemTech fellowship (3580812 Austrian Research Promotion Agency).

Author contributions

A.I.P. designed, performed and analyzed all-optical experiments. E.R. designed, performed and analyzed internal reference experiments. M.K.M., M.N., S.M.N. and M.G. designed inhibitor library and experiments and provided reagents. H.J. conceived and supervised the project and designed and analyzed experiments. A.I.P., E.R. and H.J. wrote the paper.

Competing financial interests statement

The authors declare no competing financial interests.

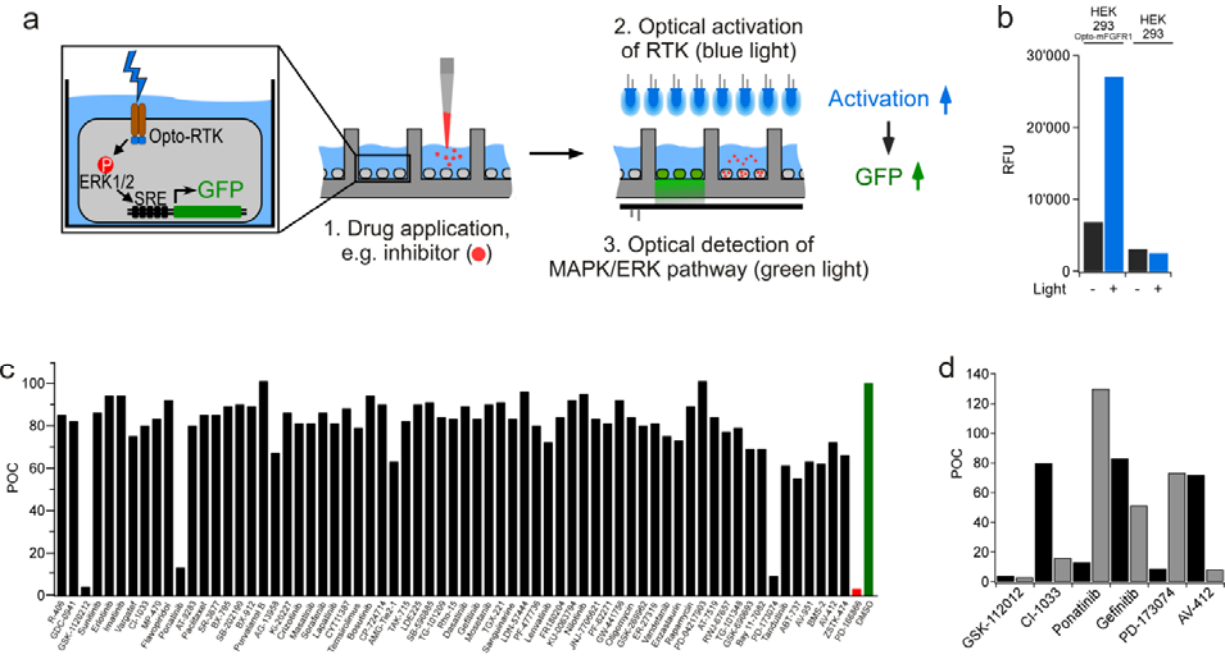
Additional information

Supplementary information is available in the online version of the paper. Reprints and permissions information is available online at <http://www.nature.com/reprints/index.html>. Correspondence and requests for materials should be addressed to H.J.

References for main text

1. Cravotto, G. & Cintas, P. *Chem. Soc. Rev.* **35**, 180-196 (2006).
2. Bradley, M. & Grieser, F. *J. Colloid. Interface Sci.* **251**, 78-84 (2002).
3. Asahi, R., Morikawa, T., Ohwaki, T., Aoki, K. & Taga, Y. *Science* **293**, 269-271 (2001).
4. Xuan, J. & Xiao, W.J. *Angew. Chem. Int. Ed. Engl.* **51**, 6828-6838 (2012).
5. Tischer, D. & Weiner, O.D. *Nat. Rev. Mol. Cell. Biol.* **15**, 551-558 (2014).
6. Szobota, S. & Isacoff, E.Y. *Annu. Rev. Biophys.* **39**, 329-348 (2010).
7. Fenno, L., Yizhar, O. & Deisseroth, K. *Annu. Rev. Neurosci.* **34**, 389-412 (2011).
8. Grusch, M. et al. *EMBO J.* **33**, 1713-1726 (2014).
9. Mohun, T., Garrett, N. & Treisman, R. *EMBO J.* **6**, 667-673 (1987).
10. Shaw, A.T., Hsu, P.P., Awad, M.M. & Engelman, J.A. *Nat Rev Cancer* **13**, 772-787 (2013).
11. Takeuchi, K. et al. *Nature medicine* **18**, 378-381 (2012).
12. Jamil, M.O., Hathaway, A. & Mehta, A. *Curr Oncol Rep* **17**, 24 (2015).
13. Shcherbo, D. et al. *Biochem J* **418**, 567-574 (2009).
14. Crouch, S.P., Kozlowski, R., Slater, K.J. & Fletcher, J. *J. Immunol. Methods* **160**, 81-88 (1993).
15. Chen, X., Wang, X., Du, Z., Ma, Z. & Yang, Y. *Curr Protoc Chem Biol* **5**, 111-129 (2013).
16. Olson, E.J., Hartsough, L.A., Landry, B.P., Shroff, R. & Tabor, J.J. *Nat Methods* **11**, 449-455 (2014).
17. Richter, F. et al. *Photochem Photobiol Sci* (2014).
18. DiNitto, J.P. et al. *J. Biochem.* **147**, 601-609 (2010).
19. Simard, J.R. et al. *J. Am. Chem. Soc.* **131**, 18478-18488 (2009).
20. Burke, P., Schooler, K. & Wiley, H.S. *Mol. Biol. Cell.* **12**, 1897-1910 (2001).
21. Toettcher, J.E., Weiner, O.D. & Lim, W.A. *Cell* **155**, 1422-1434 (2013).

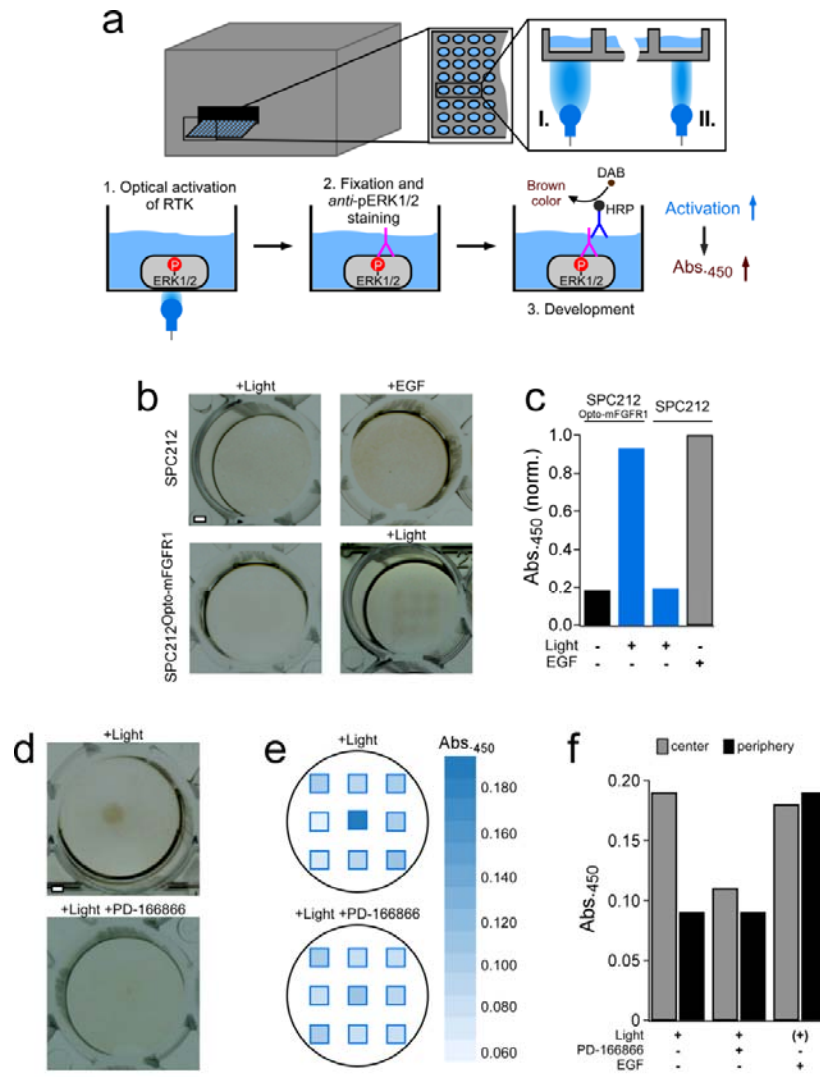
Figure legends for main text



Ingles-Prieto *et al.*
Figure 1

Figure 1. All-optical screen against RTKs and the MAPK/ERK pathway.

(a) HEK293 cells were engineered to contain an Opto-RTK (Opto-mFGFR1, Opto-hEGFR or Opto-hROS1, **Supplementary Fig. 1** and **Supplementary Fig. 8**) and a MAPK/ERK pathway-responsive GFP reporter (SRE-GFP). In all-optical screening, effects of small molecules (e.g. receptor inhibitors or pathway inhibitors) are tested in 384-well plates by first activating the RTK with blue light ($\lambda \sim 470$ nm, $I \sim 200 \mu\text{W}/\text{cm}^2$) followed by detection of pathway activity using the GFP reporter. In cells treated with inhibitors of RTKs or of components of the MAPK/ERK pathway, GFP expression will be absent. Except for small molecule addition, the process does not require contact to the cells, solution exchange or added reagents (**Supplementary Fig. 3**). (b) Control experiments demonstrating activation of MAPK/ERK pathway by Opto-mFGFR1 and blue light as measured using the GFP reporter. Mean raw fluorescent units (RFU) (one representative experiment performed in triplicate) are shown. (c) All-optical screen against mFGFR1 and MAPK/ERK pathway (68 small molecules, final concentration 5 nM). PD-166866 (final concentration 5 μM), a specific FGFR1 inhibitor, and DMSO were used as controls (red and green bars). Mean percent of control (POC) values (two independent experiments performed in duplicate) are shown. (d) Comparison of all-optical experiments with Opto-mFGFR1 (black bars) and Opto-hEGFR (grey bars) allow identifying small molecules that specifically inhibit mFGFR1 (ponatinib, PD-173074), hEGFR (CI-1033, AV-412, gefitinib) or downstream proteins of the MAPK/ERK pathway (GSK-1120212). Mean POC values (two independent experiments performed in duplicate) are shown.



Ingles-Prieto *et al.*
Figure 2

Figure 2. Optogenetics-enabled, internally-referenced measurement of MAPK/ERK pathway.

(a) Whole well (I.) or spatially-confined (II.) light stimulation ($\lambda=470 \pm 5$ nm) of SPC212^{Opto-mFGFR1} cells was performed in a microplate reader. 48-well plates were chosen for these experiments to enable visual evaluation after *anti*-pERK1/2 immunohistochemistry (see b and d). (b) Raw data photographs of cells stimulated with EGF (5.5 ng/ml) or light (distributed over the well in a 3×3 matrix). MAPK/ERK pathway was activated by EGF in SPC212 cells or light in SPC212^{Opto-mFGFR1} cells but not in controls. (c) Quantification of b. Mean (normalized) absorption values (one representative experiment with nine positions) are shown. (d) Raw data photographs of local activation (area~3.14 mm²) of the MAPK/ERK pathway by spatially-confined illumination of SPC212^{Opto-mFGFR1} cells. Activation is limited to the center of the well and inhibited by PD-166866 (final concentration 5 μ M). (e) Quantification of d. (f) Characterization of an inactive molecule (vehicle, left bars), inhibitor (PD-166866, middle bars) or activator (EGF, right bars) through internal references in a single measurement. Mean (normalized) absorption values (two independent experiments performed in triplicate or duplicate) are shown. Scale bar in b and c is 1 mm.

Online Methods

Kinase inhibitor library

Small molecules are listed in **Supplementary Table 1**. Out of the tested 68 small molecules, 62 molecules target protein kinases.

Gene constructs

Opto-mFGFR1 and Opto-hEGFR in pcDNA3.1(-) (Life Technologies) were described previously⁸. Identification of ROS1 and genetic engineering of Opto-hROS1 is described below. The SRE-GFP reporter vector and the vector containing MonsterGFP under the control of the CMV promoter were obtained from Qiagen/SA Biosciences. mKate2 was obtained from D.M. Chudakov (Shemiakin-Ovchinnikov Institute of Bioorganic Chemistry)/Evrogen¹³ and subcloned into pcDNA3.1(-) using polymerase chain reaction.

Cell culture and transfection

Malignant pleural mesothelioma SPC212 cells were kindly provided by R. Stahel (University of Zurich) and HEK293 were derived by F.L. Graham (McMaster University). Malignant pleural mesothelioma SPC212 cells stably expressing Opto-mFGFR1⁸ and HEK293 cells were maintained in RPMI1640 and DMEM, resp., in a humidified incubator with 5% CO₂ atmosphere. Media were supplemented with 10% FBS, 100 U/ml penicillin and 0.1 mg/ml streptomycin, and RPMI1640 was additionally supplemented with 2 mM L-Glutamine. For transfection of HEK293 cells, 2×10⁶ cells were seeded in 60 mm cell culture dishes coated with poly-L-ornithine (PLO, Sigma). Cells were transfected with 4.04 to 8.04 µg total DNA per dish (receptor, pcDNA3.1(-) empty vector, and reporter at a ratio of 1:50:50 or 1:100:100) using polyethylenimine (Polysciences). For mock transfected cells (**Fig. 1b** and **Supplementary Fig. 2**, "HEK293"), receptor vector was omitted in the transfection mixture. For experiments with mKate2¹³ (**Supplementary Fig. 11**), empty vector was substituted by mKate2 in pcDNA3.1(-). For control experiments with MonsterGFP (**Supplementary**

Fig. 5), reporter vector and receptor vector was substituted by vector containing MonsterGFP under the control of the CMV promoter.

Custom incubator for light stimulation of well plates

A thermoelectric incubator (PT2499, ExoTerra) was equipped with 300 RGB LEDs (5050SMD, $\lambda_{\max} \approx 630$ nm (red light), $\lambda_{\max} \approx 530$ nm (green light), $\lambda_{\max} \approx 470$ nm (blue light), bandwidth $\approx \pm 5$ nm). Light intensity was controlled with a dimmer and measured with a digital power meter (PM120VA, Thorlabs). Blue light intensity at maximal output was $247 \mu\text{W}/\text{cm}^2$. Light of this intensity is sufficient for activation and well tolerated by mammalian cells without signs of toxicity even for extended periods of time. Hardware to maintain a CO_2 atmosphere is not required if medium supplemented with HEPES (25 mM) is used during light stimulation (see below). To measure profile of light distribution, the sensor of the power meter was mounted on a holder and moved in 1 cm steps. Intensity was recorded and deviation between highest and lowest intensity was calculated ($\Delta < 0.13 \mu\text{W}/\text{cm}^2$). Day-to-day variability of light was measured in the same way but on several days distributed over one week ($\Delta < 0.13 \mu\text{W}/\text{cm}^2$). For evaluation of the effect of ambient light (**Supplementary Fig. 4**), cells were stimulated immediately after seeding with white light of comparable intensity to that encountered in a dim room.

All-optical drug screening against RTKs and the MAPK/ERK pathway

The workflow is depicted in **Supplementary Fig. 3**. Transfected HEK293 cells were kept in DMEM (supplemented with 5% FBS and no antibiotics; “D5-AB” medium) for 6 h. Afterwards, 5'000 to 20'000 cells were seeded in each well of 384-well plates (3712, Corning) in low-fluorescence medium (FlouoBrite™, Life Technologies, supplemented with 25 mM HEPES, 0.5% FBS, 100 U/ml penicillin and 0.1 mg/ml streptomycin, pH 7.5; “COI” medium). Small molecules were added and after 1 h cells were stimulated with blue light in a custom incubator (see above). Unstimulated cells were kept in the dark by covering selected wells on the same 384-well plate. GFP fluorescence was then measured in a microplate reader (Synergy H1, BioTek) at the optimized excitation wavelength

of 500 ± 5 nm and emission wavelength of 535 ± 5 nm (10 measurements per well, measurement duration: 10 ms, gain: 90 to 130). We found that 384-well plates exhibit fluorescence in the blue-green part of the light spectrum (**Supplementary Fig. 11**), and optimization of the excitation wavelength allowed for improved signal to noise ratio. mKate2 fluorescence was measured at excitation wavelength of 570 ± 5 nm and emission wavelength of 660 ± 5 nm.

Identification of Orphan RTKs

Orphan RTKs were identified using the bioinformatics procedure described in **Supplementary Fig. 7**. Protein family search with the PFAM motif “Pkinase_Tyr” (PF07714) at the Wellcome Trust Sanger Institute (<http://pfam.xfam.org/>)²² retrieved a comprehensive list of human Tyr kinases. This PFAM motif is a good representative of kinase domains found in RTKs (we confirmed that it is found in members of diverse RTK families, such as fibroblast growth factor receptors, ErbB receptors, Insulin-like growth factor receptor, neurotrophin receptors, ROR receptors). Retrieval of these sequences was followed by transmembrane helix prediction with TMHMM²³ to retain only sequences with transmembrane helices. To remove sequence redundancy and assign sequence fragments clustering with UCLUST²⁴ was performed. 69 clusters with a unique candidate sequence each for RTKs were obtained **Supplementary Table 2** and orphan RTKs were identified by manual curation.

Genetic engineering of Opto-ROS1

A sequence coding for the ROS1 gene was obtained from the Mammalian Gene Collection (Dharmacon, GE Life Science). Using inverse PCR, an expression vector was prepared starting from an Opto-mFGFR1 vector in which the mFGFR1 ICD was replaced by two inverted SapI restriction sites. The ROS1 ICD was amplified with oligonucleotides (F: GAT CGC TCT TCA GAC CAT AGA AGA TTA AAG AAT CAA AAA AG, R: GAT CGC TCT TCC AGG ATC AGA CCC ATC TCC ATA TCC ACT G) and PCR and inserted into the vector using ‘Golden Gate’ cloning²⁵.

Activation of Opto-RTKs in microplate reader and ERK1/2 phosphorylation

5×10^4 cells per well were seeded in 48-well plates coated with PLO and starved for 24 h in medium containing 0.1% FBS. Small molecules or EGF (5.5 ng/ml) were added to the cells one h prior to onset of light stimulation. A microplate reader equipped with monochromators (Synergy H1, BioTek; 9 W average power of flash lamp, 2 μ s flash duration) was repurposed for spatially-confined light stimulation and read-out. For stimulating entire wells, the device's area scanning mode was configured for a 3 \times 3 matrix with horizontal and vertical point spacing of 2 mm. This protocol was repeated 100 times. For stimulating well centers, the device's area scanning mode was configured for a 9 \times 9 matrix with minimal point spacing. This protocol was repeated three times. In both protocols, bottom illumination at an excitation wavelength of 470 nm was applied. Cells were then fixed and permeabilised in a solution containing 4% formaldehyde and 1% methanol for 15 min. After washing with PBS three times for 5 min, cells were blocked in 1% BSA, 0.1% Tween in PBS for 30 min and incubated with anti-pERK1/2 (#9101, Cell Signaling Technology, 1:500) for 1 h. After washing with PBS three times for 5 min, signal was developed using the UltraVision LP detection system (Thermo Scientific) and 3,30-diaminobenzidine as chromogen. For read-out, the device's area scanning mode was configured for a 3 \times 3 with spacing of 3 mm. In some experiments, this protocol was repeated three times with absorbance measurements at 450 nm. Data were normalized to EGF-treated wells and background (SPC212 cells in the dark) was subtracted. Photographs were acquired with a macroscope²⁶. This approach can also be used for blue light activation of gene transcription using a different optogenetic system (see below).

Optimization of excitation wavelength for microplate reader GFP measurements

The microplate reader was used to quantify fluorescence of 384-well plates filled with low-fluorescence media. Emission spectra were acquired at several fixed excitation wavelengths (**Supplementary Fig. 12**).

Assay validation and statistical analysis

Z' factors (**Supplementary Table 3**) were calculated for interleaved-signal format plates following

$$Z' factor = 1 - \frac{3 \times (std(c_+) + std(c_-))}{|avg(c_+) - avg(c_-)|}$$

where $std(c_+)$ and $avg(c_+)$ are the standard deviation and the average of DMSO treated samples, resp., and $std(c_-)$ and $avg(c_-)$ are the standard deviation and the average of PD-166866 (INH; final concentration 20 μ M) treated samples, resp. On each plate, ten columns of DMSO treated samples and ten columns of INH treated samples were tested in groups of two and in alternating order). Z' factors for these plates were ≥ 0.70 (**Supplementary Table 3**) and failures were not observed. Percentage of control (POC) values were calculated following:

$$POC = \frac{X_i}{avg(c_+)} \times 100$$

where X_i is the measurement of the i^{th} small molecule and $avg(c_+)$ is the average measurement of the DMSO treated samples.

Methods-only References

22. Finn, R.D. et al. *Nucleic Acids Res.* **38**, D211-222 (2010).
23. Krogh, A., Larsson, B., von Heijne, G. & Sonnhammer, E.L. *J. Mol. Biol.* **305**, 567-580 (2001).
24. Edgar, R.C. *Bioinformatics* **26**, 2460-2461 (2010).
25. Engler, C. & Marillonnet, S. *Methods Mol Biol* **1116**, 119-131 (2014).
26. Chait, R., Shrestha, S., Shah, A.K., Michel, J.B. & Kishony, R. *PLoS One* **5**, e15179 (2010).

Light-assisted small molecule screening against protein kinases

Álvaro Inglés-Prieto¹, Eva Reichhart¹, Markus K. Muellner², Sebastian M. Nijman^{2,4}, Michael Grusch³ & Harald Janovjak^{1,*}

¹ Institute of Science and Technology Austria (IST Austria), 3400 Klosterneuburg, Austria.

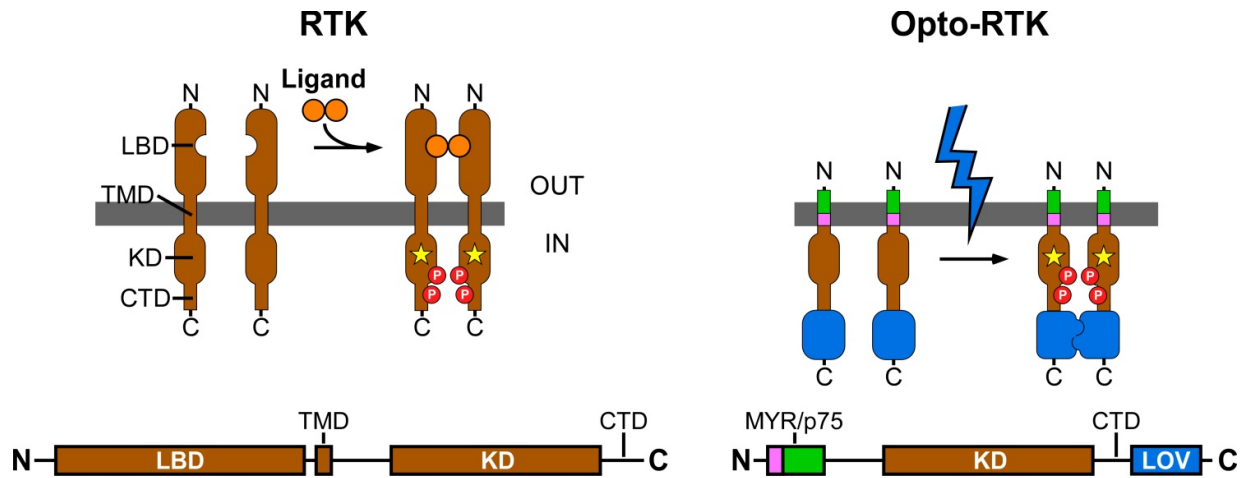
² CeMM-Research Center for Molecular Medicine of the Austrian Academy of Sciences, 1090 Vienna, Austria.

³ Institute of Cancer Research, Department of Medicine I, Comprehensive Cancer Center Vienna, Medical University of Vienna, 1090 Vienna, Austria.

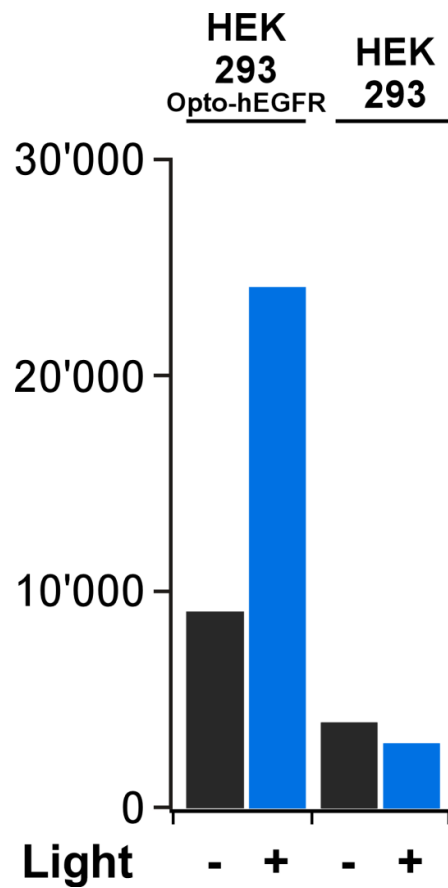
⁴ Present address: Ludwig Institute for Cancer Research, NDM Research Building, Roosevelt Drive, Headington, Oxford OX3 7XR, United Kingdom.

*e-mail: harald@ist.ac.at

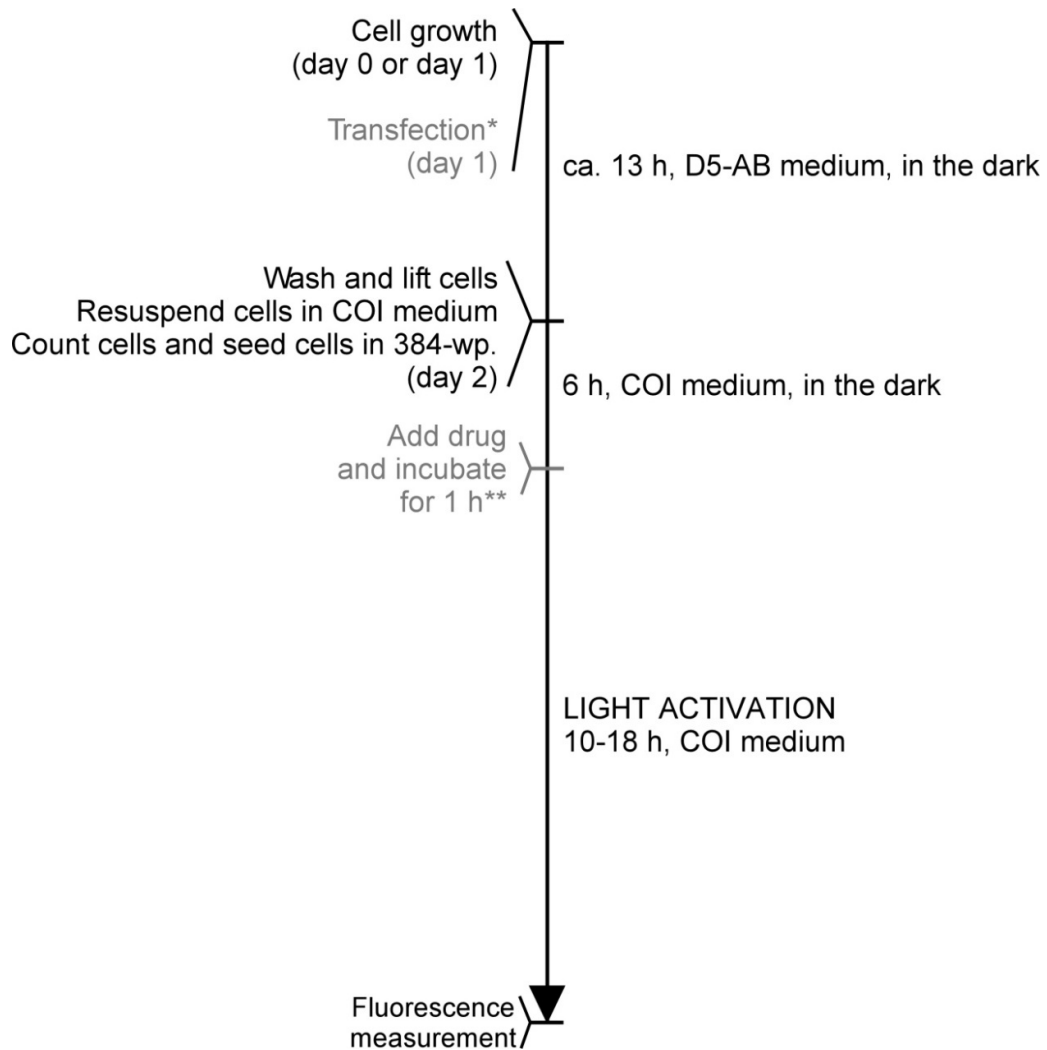
Supplementary Results



Supplementary Figure 1: Design and function of Opto-RTKs. RTKs consist of an extracellular ligand-binding domain (LBD), single-span transmembrane domain (TMD) and intracellular domain (ICD), which includes the kinase domain (KD) and a C-terminal tail domain (CTD). In Opto-RTKs (e.g. Opto-mFGFR1 or Opto-hEGFR¹), only the ICD is retained to render the protein insensitive to endogenous ligands. The ICD is attached to the membrane using a myristoylation domain (MYR; for mFGFR1) or the extracellular and transmembrane domain of the p75 low-affinity neurotrophin receptor (p75; for hEGFR). The light-oxygen-voltage-sensing (LOV) domain from aureochrome1 of the algae *Vaucheria frigida* is incorporated at the ICD C-terminus and induces homodimerization upon blue light stimulation. Except for MYR and p75, domains are drawn to scale (length of amino acid sequences).

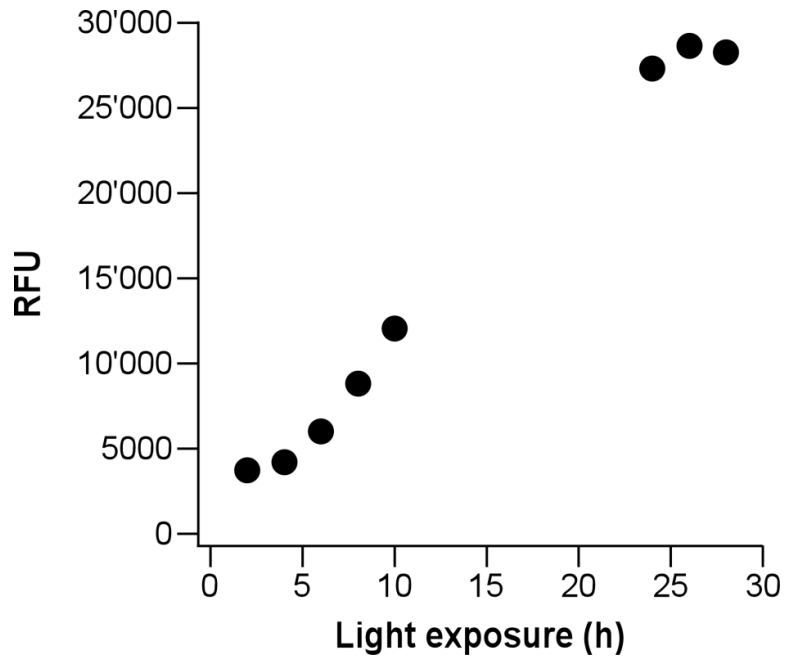


Supplementary Figure 2: Activation of MAPK/ERK pathway by Opto-hEGFR. Activation was measured using SRE-GFP after 18 h and is represented as raw fluorescence units (RFU). Mean values (two independent experiments performed in duplicate) are shown.

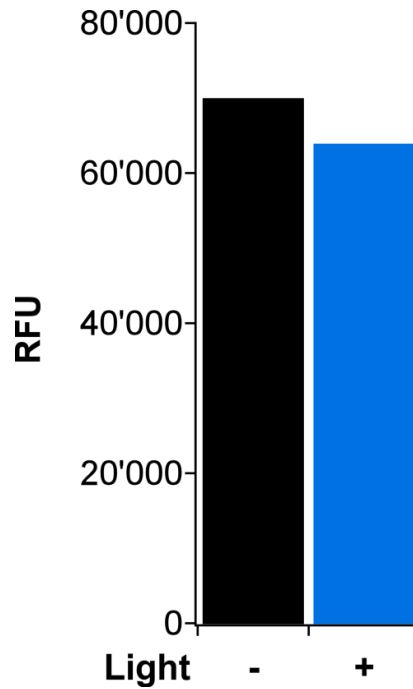


Supplementary Figure 3: Workflow of the all-optical screen method (compare to Fig. 1).

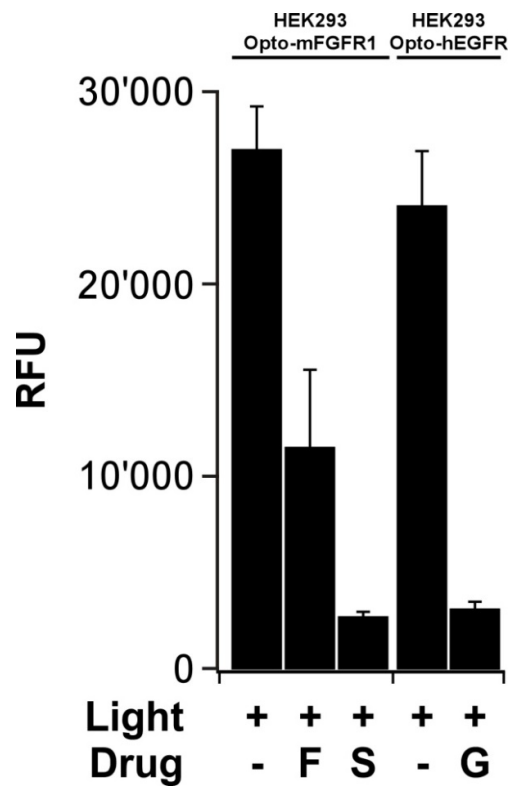
*Transfection can be omitted when a stable cell line is used. **Drug addition can be performed at the beginning of the workflow by preparing drugs in the 384-well plates. Media are described in **Materials and Methods**.



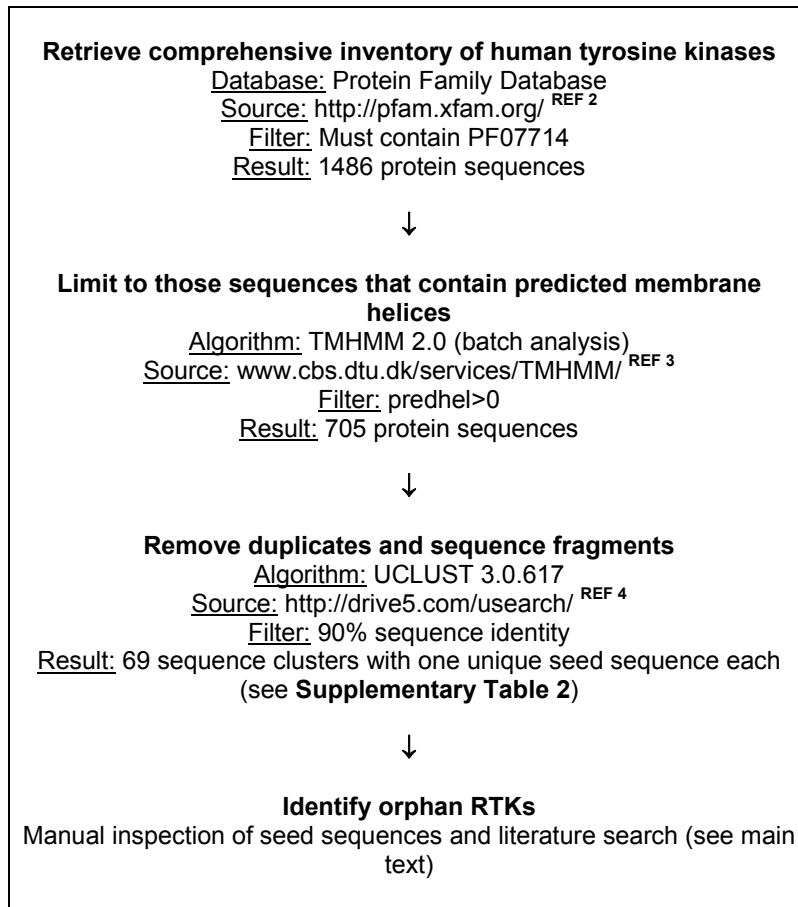
Supplementary Figure 4: Opto-RTK activation by room light. HEK293 cells transfected with Opto-mFGFR1 and SRE-GFP were exposed to dimmed white laboratory light (intensity $\sim 30 \mu\text{W}/\text{cm}^2$). To analyze MAPK/ERK pathway activation, fluorescence was measured every hour. An increase in reporter signal is detected for illumination duration exceeding 4 h. Mean raw fluorescence units (RFU) (one representative experiment performed in eight wells) are shown.



Supplementary Figure 5: Bleaching of GFP by stimulation light. MonsterGFP, which is the fluorescent protein employed in the reporter plasmid, was expressed in HEK293 cells under the control of the constitutively active CMV promoter. Cells were stimulated with light following the standard protocol (**Fig. 1** and **Supplementary Fig. 3**) to test if stimulation light bleaches GFP. Bleaching <10% was detected. Mean raw fluorescence units (RFU) (one representative experiment performed in 96 wells) are shown.

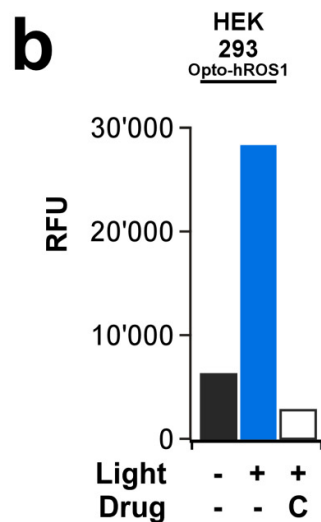
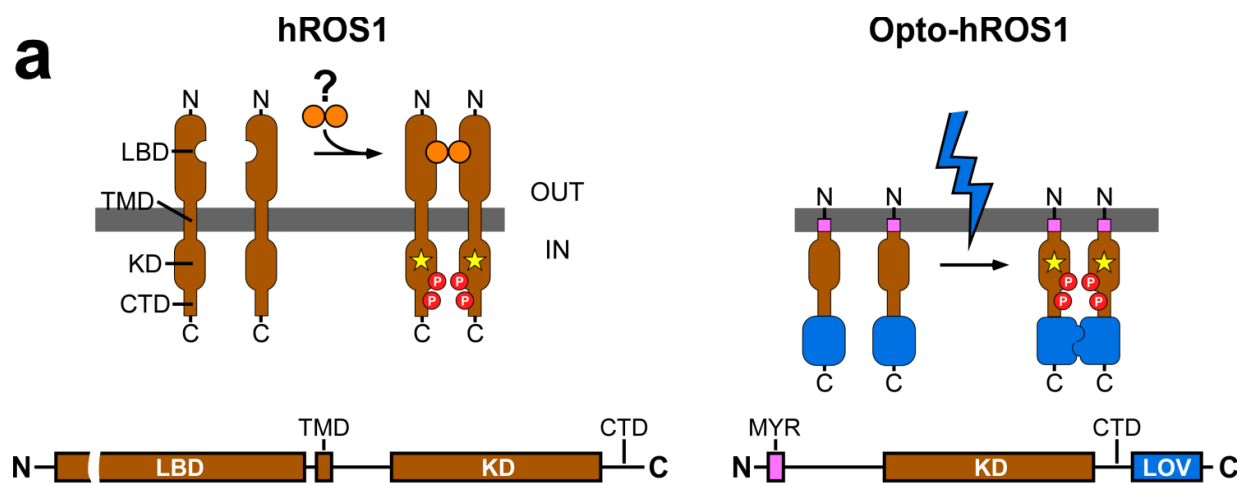


Supplementary Figure 6: Inhibition by FR180204 (F), sorafenib (S), and gefitinib (G) (final concentration 10 μ M). Mean raw fluorescence units (RFU) \pm SEM (three independent experiments performed in duplicate) are shown.

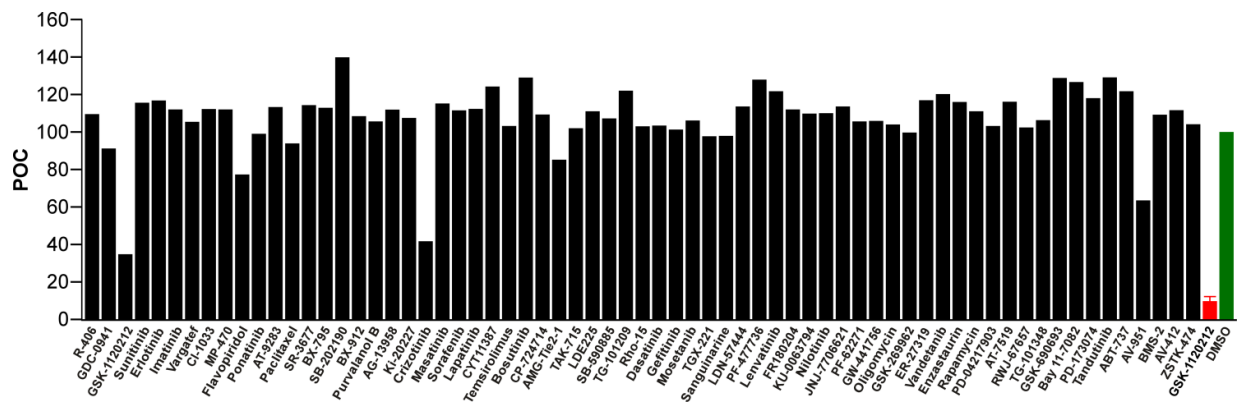


Supplementary Figure 7: Bioinformatics procedure for identification of orphan RTKs.

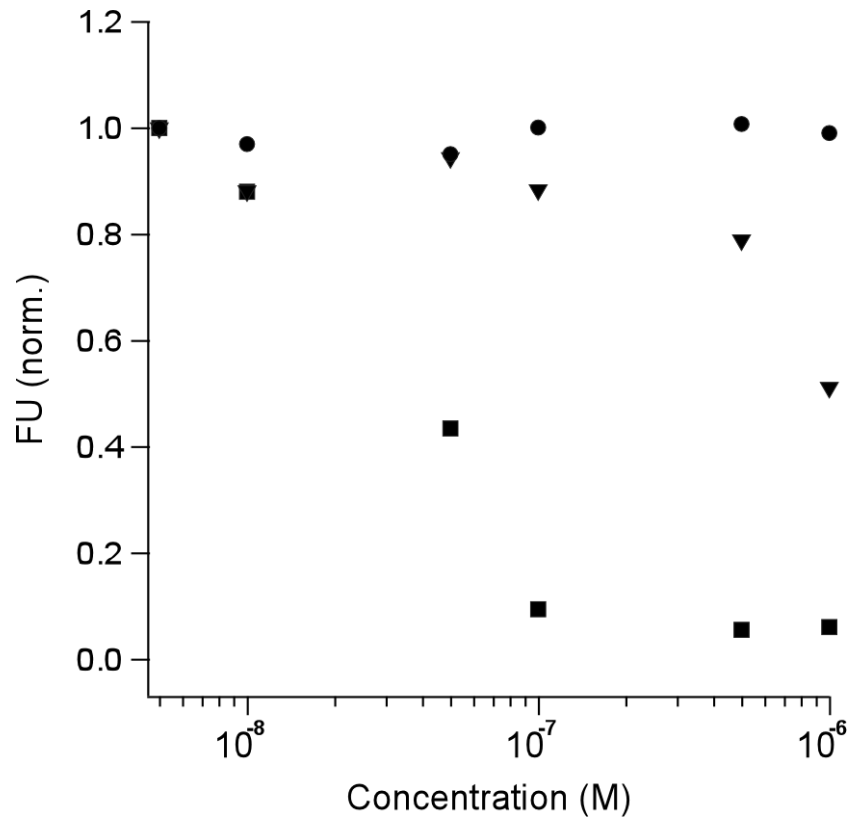
Individual steps are described in the **Materials and Methods** section. Databased search was conducted June 2014.



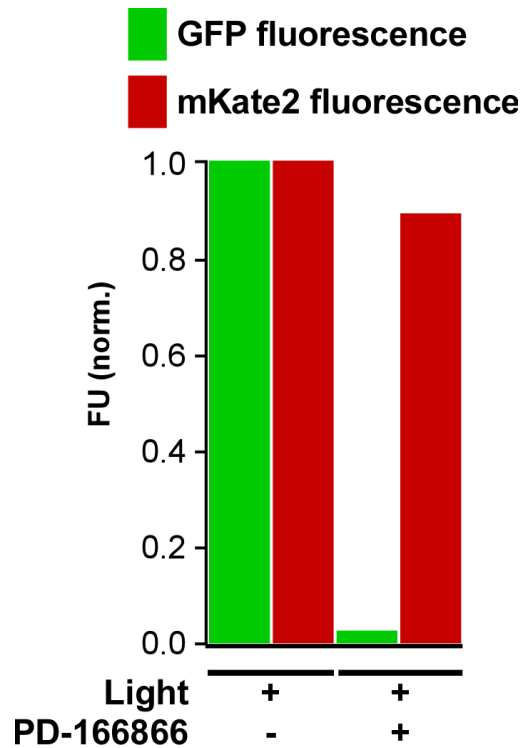
Supplementary Figure 8: Light activation of an orphan RTK. (a) The orphan RTK hROS1 was re-engineered to be activated by light by fusing its cytosolic domain to the dimerizing LOV domain. Except for ECD of hROS1, domains are drawn to scale (length of amino acid sequences). (b) Control experiments demonstrating activation of MAPK/ERK pathway by Opto-hROS1 and specific inhibition by crizotinib (C; final concentration 100 nM). Mean raw fluorescence units (RFU) (one representative experiment performed in triplicate) are shown.



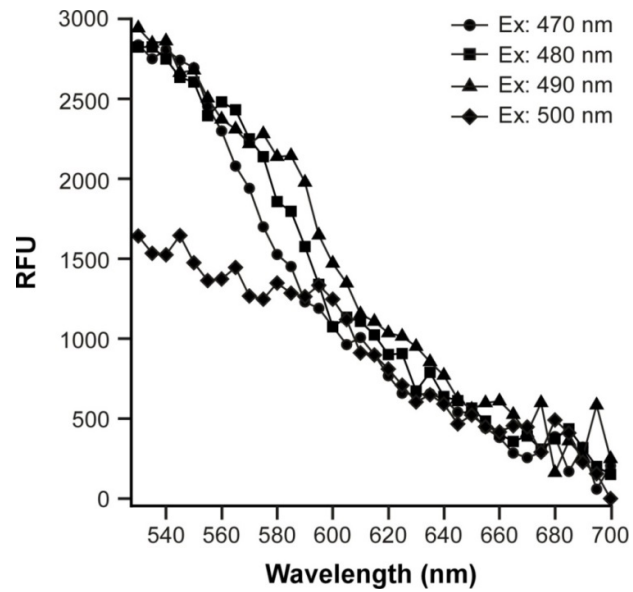
Supplementary Figure 9: All-optical screen against hROS1 and MAPK/ERK pathway. The screen contained the same 68 small molecules as in **Fig. 1** (final concentration 100 nM). GSK-1120212 (final concentration 1 μM) and DMSO were used as controls (red and green bars). Mean percent of control (POC) values (two independent experiments performed in duplicate) are shown.



Supplementary Figure 10: Inhibition of the hROS1-MAPK/ERK-axis (squares), mFGFR1-MAPK/ERK-axis (triangles) and EGFR-MAPK/ERK-axis (spheres) by increasing doses of AV-951. Mean normalized (to datapoint with the highest intensity in each experiment) fluorescence units (FU) (two independent experiments performed in eight wells each) are shown.



Supplementary Figure 11: Simultaneous measurement of disruption of transcription and translation. The red fluorescent protein mKate2 extends all-optical experiments with a measurement of disruption of transcription and translation. mKate2, SRE-GFP and Opto-mFGFR1 were co-expressed in HEK293 cells and stimulated with light as described for **Fig. 1**. Expression of mKate2 was under the control of the constitutively active CMV promoter and is thus mainly sensitive to disruption of transcription and translation. Incubation with PD-166866 indicates reduced MAPK activity specifically and demonstrates that the two fluorescent proteins can be detected separately. Mean normalized (to measurements without inhibitor) fluorescence units (FU) (two independent experiments performed in duplicate) are shown.



Supplementary Figure 12: Background fluorescence of 384-well plates filled with COI medium. Fluorescence emission spectra of single wells filled with low-fluorescence media were recorded for four excitation wavelengths between 470 and 500 nm (± 5). Excitation wavelength of 500 ± 5 nm was selected for experiments because of the low background fluorescence (one representative experiment).

Supplementary Table 1: Small molecules used in this manuscript along with POC inhibition of the mFGFR1-MAPK/ERK-axis.

Small molecule	Canonical target(s)	Source	POC (Fig. 1c)
R-406	Syk	MedChem Express	85
GDC-0941	PI3K α/δ	Selleck	82
GSK-1120212	MEK1/2	Selleck	4
Sunitinib	VEGFR2, PDGFR β , c-Kit	Synthesis	86
Imatinib	v-Abl, c-Kit, PDGFR	Selleck	94
Erlotinib	EGFR	Synthesis	94
Vargatef	VEGFR1/2/3, FGFR1/2/3, PDGFR α/β	Synthesis	75
CI-1033	EGFR, ErbB2	Selleck	80
MP-470	c-Kit, PDGFR α , Flt3	Selleck	83
Flavopiridol	CDK1/2/4/6, EGFR, PKA	Santa Cruz	92
Ponatinib	Abl, PDGFR α , VEGFR2, FGFR1, Src	ARIAD	13
AT-9283	JAK2/3	Selleck	80
Paclitaxel	Microtubule polymer stabilizer	Sigma	85
SR-3677	ROCK2	Sigma	85
BX-795	PDK1	Selleck	89
SB-202190	p38 α/β	Selleck	90
BX-912	PDK1	Selleck	89
Purvalanol B	CDC2, CDK2/4/5	Tocris	101
AG-13958	VEGF	Synkinase	67
Ki-20227	c-Fms, VEGFR2, PDGFR β , c-Kit	APExBio	86
Crizotinib	c-Met, ALK	APExBio	81
Masatinib	Abl, Src, c-Kit,	Synthesis	81
Sorafenib	Raf-1, B-Raf, VEGFR-2	Synthesis	86
Lapatinib	EGFR, ErbB2	Synthesis	81
CYT11387	JAK1/2	Synthesis	88
Temsirolimus	mTOR	Selleck	79
Bosutinib	Src, Abl	Synthesis	94
CP-724714	ErbB2	Selleck	90
AMG-Tie2-1	Tie-2	Synkinase	63
TAK-715	p38 α	Selleck	82
LDE225	SMO	Selleck	90
SB-590885	B-Raf	APExBio	91
TG-101209	JAK2, Flt3, RET	Selleck	84
Rho-15	ROCK1/2	Synthesis	83
Dasatinib	Abl, Src, c-Kit	Synthesis	89
Gefitinib	EGFR	Synthesis	83
Mosetanib	VEGFR1/2/3	Synthesis	90
TGX-221	p110 β	Selleck	91
Sanguinarine	Na ⁺ /K ⁺ -and Mg ²⁺ -ATPase inhibitor	Santa Cruz	83
LDN-57444	Proteasome inhibitor for Uch-L1	Selleck	96
PF-477736	Chk1, VEGFR2, Aurora-A, FGFR3, Flt3, Fms, Ret, Yes	Sigma	80
Lenvatinib	VEGFR2/3/1, FGFR1, PDGFR α/β	Source	72

FR180204	ERK1/2	MedChem Express	84
KU-0063794	mTORC1/2	Selleck	92
Nilotinib	Bcr-Abl	Selleck	95
JNJ-7706621	CDK1/2, Aurora A/B	Synthesis	83
PF-62271	FAK, Pyk2	Selleck	81
GW-441756	TrkA	Synthesis	92
Oligomycin	ATP synthase	Synthesis	84
GSK-269962	ROCK1/2	Selleck	80
ER-27319	Syk	Selleck	81
Vandetanib	VEGFR2	Santa Cruz	75
Enzastaurin	PKC β / α / γ / ϵ	ARIAD	73
Rapamycin	mTOR	Selleck	89
PD-04217903	c-Met	Sigma	101
AT-7519	CDK1/2/4/6/9	Sigma	84
RWJ-67657	p38 α / β	Selleck	77
TG-101348	JAK2/1/3, BRD4	Selleck	79
GSK-690693	Akt1/2/3, PKA, PrkX, PKC	Selleck	69
Bay 11-7082	NF- κ B, I κ B α	Tocris	69
PD-173074	FGFR1	Synkinase	9
Tandutinib	FLT3, PDGFR, c-Kit	APExBio	61
ABT-737	Bcl-xL, Bcl-2, Bcl-w	APExBio	55
AV-951	VEGFR1/2/3, PDGFR, c-Kit	Synthesis	63
BMS-2	c-Met	Synthesis	62
AV-412	EGFR, ErbB2	Synthesis	72
ZSTK-474	PI3K δ	Synthesis	66
PD-166866	FGFR1	Selleck	3

Supplementary Table 2: Seed sequences retrieved using the bioinformatics procedure described in Supplementary Fig. 8. Where necessary for clarity, gene short names were added in square brackets to the Uniprot description column. Stars (*) denote RTKs identified as orphans.

Uniprot-ID	Uniprot Description
D7RF68	AGTRAP-BRAF fusion protein
Q59HE0	Colony stimulating factor 1 receptor variant
Q6P4R6	EPH receptor A3
Q7Z635	EPH receptor B4
B7ZKW7	EPHA5 protein
Q4LE53	EPHB2 variant protein
P21709	Ephrin type-A receptor 1
E7EML7	Ephrin type-A receptor 10
P29317	Ephrin type-A receptor 2
P54764	Ephrin type-A receptor 4
Q9UF33	Ephrin type-A receptor 6
D6RAL5	Ephrin type-A receptor 6
P29322	Ephrin type-A receptor 8
P54762	Ephrin type-B receptor 1
P29323	Ephrin type-B receptor 2
P54753	Ephrin type-B receptor 3
O15197	Ephrin type-B receptor 6
A2ABM8	Epithelial discoidin domain-containing receptor 1
E7EU09	Fibroblast growth factor receptor [FGFR1]
D3DRD5	Fibroblast growth factor receptor [FGFR2]
F8W9L4	Fibroblast growth factor receptor [FGFR3]
P22607	Fibroblast growth factor receptor 3
Q59F30	Fibroblast growth factor receptor 4 variant
P25092	Heat-stable enterotoxin receptor
P08581	Hepatocyte growth factor receptor
B2RE75	Highly similar to Homo sapiens c-mer proto-oncogene tyrosine kinase (MERTK)
A8K2T7	Highly similar to Homo sapiens epidermal growth factor receptor (erythroblastic leukemia viral (v-erb-b) oncogene homolog avian) (EGFR)
A8KAM8	Highly similar to Homo sapiens platelet-derived growth factor receptor betapolyptide (PDGFRB)
E9PFZ5	Inactive tyrosine-protein kinase 7
P06213	Insulin receptor
P14616	Insulin receptor-related protein
P08069	Insulin-like growth factor 1 receptor
Q59EB0	Kinase insert domain receptor (A type III receptor tyrosine kinase) variant [VEGFR2]
P29376	Leukocyte tyrosine kinase receptor
P07333	Macrophage colony-stimulating factor 1 receptor
Q04912	Macrophage-stimulating protein receptor
P10721	Maststem cell growth factor receptor Kit
F5H3K9	Muscle skeletal receptor tyrosine-protein kinase
Q16288	NT-3 growth factor receptor
P16234	Platelet-derived growth factor receptor alpha

Q9H5K3*	Protein kinase-like protein SgK196
P08922*	Proto-oncogene tyrosine-protein kinase ROS
Q6MZT2	Putative uncharacterized protein DKFZp686D1354 [DDR2]
A1L4F5	Receptor tyrosine kinase-like orphan receptor 2 [ROR2]
P04626	Receptor tyrosine-protein kinase erbB-2
P21860	Receptor tyrosine-protein kinase erbB-3
Q15303	Receptor tyrosine-protein kinase erbB-4
Q5VTU6	Receptor-type tyrosine-protein kinase FLT3
F8TLW0	Ret proto-oncogene tyrosine-protein kinase receptor isoform a
Q02846	Retinal guanylyl cyclase 1
P51841	Retinal guanylyl cyclase 2
Q8IWU2	Serinethreonine-protein kinase LMTK2
Q96Q04	Serinethreonine-protein kinase LMTK3
Q59HG2	TEK tyrosine kinase variant
Q59FM9	TYRO3 protein tyrosine kinase variant
Q15516	Tyrosine kinase [Mer variant]
F8WED1	Tyrosine-protein kinase Mer
F0UY65	Tyrosine-protein kinase receptor [Alk]
A9YLN4	Tyrosine-protein kinase receptor [CD4-ROS1 fusion]
A9YLN5	Tyrosine-protein kinase receptor [SLC34A2-ROS1 fusion]
A8K3Z4	Tyrosine-protein kinase receptor [trkA]
Q548C2	Tyrosine-protein kinase receptor [trkB]
P35590	Tyrosine-protein kinase receptor Tie-1
F5H4Q1	Tyrosine-protein kinase receptor TYRO3
P30530	Tyrosine-protein kinase receptor UFO
P34925	Tyrosine-protein kinase RYK
Q6J9G0*	Tyrosine-protein kinase STYK1
A2VCQ3	Tyrosine-protein kinase transmembrane receptor ROR1
P35916	Vascular endothelial growth factor receptor 3

Supplementary Table 3: Statistical analysis of assay data. Statistics were determined for interleaved-format plates (each plate contained ten columns for DMSO and ten columns for INH with alternating order; also see **Materials and Methods**).

Plate	Statistics
Day 1, Plate 1	Mean (DMSO) 40756 SD (DMSO) 3689 Mean (INH) 1217 SD (INH) 271 Z' 0.70
Day 1, Plate 2	Mean (DMSO) 42404 SD (DMSO) 3925 Mean (INH) 1225 SD (INH) 269 Z' 0.69
Day 2, Plate 1	Mean (DMSO) 60338 SD (DMSO) 5068 Mean (INH) 1632 SD (INH) 341 Z' 0.72
Day 2, Plate 2	Mean (DMSO) 53434 SD (DMSO) 4865 Mean (INH) 1599 SD (INH) 318 Z' 0.70

References

1. Grusch, M. et al. *EMBO J.* **33**, 1713-1726 (2014).
2. Finn, R.D. et al. *Nucleic Acids Res.* **42**, D222-230 (2014).
3. Krogh, A., Larsson, B., von Heijne, G. & Sonnhammer, E.L. *J. Mol. Biol.* **305**, 567-580 (2001).
4. Edgar, R.C. *Bioinformatics* **26**, 2460-2461 (2010).